ELSEVIER

Biophysical Chemistry 82 (1999) 83–97

Biophysical Chemistry

www.elsevier.nl/locate/bpc

Looking inside molecular bonds at biological interfaces with dynamic force spectroscopy

Evan Evans[a,b,*]

[a] *Departments of Physics and Pathology, University of British Columbia, Vancouver, BC, Canada V6T 1Z1*
[b] *Department of Biomedical Engineering, Boston University, Boston, MA 02215, USA*

Received 15 September 1999; accepted 15 September 1999

Abstract

Weak non-covalent interactions between large molecules govern interfacial structure and adhesion in biology. Because of thermal activation, these bonds have modest lifetimes and bond lifetimes are progressively shortened under application of external force. Theory predicts that bond survival time depends on how fast the force is applied and the expected survival time specifies the most likely breakage force (strength) at a given loading rate (force/time). Plotted as a function of $\log_e$ (loading rate), the dynamic spectrum of bond strength provides an image of the prominent barriers traversed in the energy landscape along the unbinding pathway, which establishes a direct link between measurements of bond force and molecular-scale chemistry. Experimentally, the challenge is to measure bond strength over several orders of magnitude in loading rate. With a recently designed probe technique, we have measured strengths of single receptor–ligand bonds and receptor-membrane anchoring over an enormous range of loading rates from 10^{-1} pN/s to 10^{5} pN/s, which reveals an inner view of the complexity of these interactions.

Keywords: Energy landscapes of biomolecular bonds; Dynamic force spectroscopy; Receptor–ligand interactions; Receptor-membrane anchoring.

1. Introduction

When we test strength of bonds at surfaces, we determine the maximum force that a molecular attachment can support at the instant of failure. Unlike covalent connections within protein and lipid molecules, interfacial structure and adhesion in biology involve non-covalent interactions between large macromolecules, which have limited lifetimes and thus will fail under any level of force if pulled on for the right length of time.

* *E-mail address:* evans@physics.ubc.ca (E. Evans)

0301-4622/99/$ - see front matter
PII: S0301-4622(99)00108-8

In referring to strength, we should think of the force that is most likely to disrupt an adhesive bond or structural linkage on a particular time scale. At equilibrium, bonds dissociate and reform under zero force which shows that an isolated bond has no strength on time scales longer than its natural lifetime for spontaneous (entropy-driven) dissociation. On the other hand, if detached in less time than needed for diffusive relaxation over the range of interaction, bond strength will reach and may even exceed the maximum gradient in a potential of mean force ($\sim$ interaction energy/bond length). Between slow spontaneous transition (μs to months) and ultrafast diffusive relaxation ($<$ ns), bond lifetime and rupture strength under external force are intimately tied together by thermally-activated kinetics in a way that depends on how the force is applied over time. Since application of force always requires a finite interval of time, the simplest way to parameterize loading is to treat force as a ramp in time set by a constant loading rate (which is what single molecular attachments experience in most force probe experiments). Based on this parameterization and well-known physics of Brownian kinetics in liquids, we have shown that bond breakage occurs most frequently at a time and force set by the loading rate [1]. Of particular significance, the continuous plot of most likely rupture force (strength) expressed on a scale of $\log_e$ (loading rate) images the most prominent barriers traversed in the energy landscape along the force-driven pathway. In this way, *dynamic force spectroscopy* DFS can be used to probe the inner world of molecular-scale chemistry but bond strengths have to be measured over many orders of magnitude in loading rate. Recently, we've explored the capability of this method to test diverse types of molecular linkages [2–4]. With a rather simple force probe, we have measured dynamic strength spectra for two receptor–ligand bonds [biotin-(strept)avidin and carbohydrate-L selectin] and receptor–lipid anchoring to membranes over an enormous span in loading rate from <0.1 pN/s to $\sim 10^5$ pN/s. More important than demonstrations of technique, the spectra show that a cascade of sharp energy barriers exists in these unrelated receptor–ligand bonds where each barrier governs strength on a different time scale and that anchoring of receptors to surface structure plays an important role in adhesion strength. Taken together, the results provide a new level of insight into the complexity of macromolecular interactions and expose the unexpected impact of force on biochemical kinetics.

2. Testing bond strength with force probes

Before reviewing the theoretical basis of the DFS method, it is instructive to first consider what is actually measured in laboratory tests of bond strength. In probing bonds, experimentalists often expect that force measurements will establish a well-defined property of an interaction between molecules. The anticipated outcome stems from the concept that strength is the maximum gradient $-(\partial E/\partial x)_{\max}$ of an interaction potential or energy contour $E(x)$ defined along the direction (x) of separation. Hence, a bond should only break once force exceeds the ratio of bond energy to the effective bond length. However, as seen below, the surprise is that even bonds with large binding energies can fail under minuscule forces — more than 100-fold lower than the maximum energy gradient implied by energy/distance. Moreover, measurements of bond forces — no matter how precise the technique or carefully performed — always yield a spread in values and the most frequent value of force depends on how fast the bonds are loaded.

With few exceptions, tests of bond strength follow a generic approach. In the procedure, a probe decorated with a small amount of ligand — and a substrate studded with specific receptors — are repeatedly touched together through steady precision movement to/from contact (Fig. 1 shows the biomembrane force probe BFP [5] that we use to test bond strength). If the surfaces are prepared with a sufficiently low density of reactive sites and embedded in a matrix of steric repellers to eliminate non-specific attachments, point contacts between the probe tip and the test surface occasionally produce specific attachments (e.g. one bonding event for every 5–10 touches). Un-

der controlled touch, infrequent attachment ensures a high probability for formation of single bonds ($\sim 95\%$ confidence when one attachment occurs out of 10 touches). After attachment, the force transducer exhibits an extension or deflection during surface separation. Bond rupture is signalled by rapid recoil at breakage and the rupture force is given by the maximum transducer extension Δx_t, i.e. $\mathbf{f} = k_f \Delta x_t$, where k_f is the spring constant of the transducer. After many hundreds of touches, detachment forces are then cumulated into a histogram. The peak in the distribution is the most likely rupture force that defines bond strength. Accepting that attachments are held only by single bonds, the subtle feature of the generic method is that the force experienced by an attachment is not constant but increases in time. In Fig. 2, this is shown by traces of force vs. time prior to rupture of single receptor–ligand bonds. The linear rise of force with time is set by the product of separation speed v_t and transducer spring constant k_f, which is called the loading rate $r_f = k_f v_t$. (Note: if soft structures like long polymers link the bond to a stiff probe, the loading history can be non-linear in time [6].) Very different levels of force and time span characterize the detachment processes seen in Fig. 2. Comparing these, it is clear that bond survival and detachment force depend on the rate of loading in reciprocal ways: i.e. under high speed loading, the attachment has a short lifetime but withstands a large force whereas under low speed loading, the attachment has long lifetime but only sustains a small force. The theory presented in the next section shows that this reciprocity stems from thermally-activated kinetics.

Two unrelated pairs of receptor–ligand molecules were probed with the BFP technique. In the first set of tests [2], bonds were formed between the ligand, biotin (a vitamin) and the protein receptor, streptavidin (from bacteria) or the closely similar protein avidin (from hen egg white). Used widely in biotechnology, this molecular pair represents one of the highest affinity non-covalent bonds in biology [7] with a force-free lifetime on the order of days [8]. In the second set of tests [3], bonds were formed between a sialylated (carbohydrate) short peptide ligand and the L-selectin receptor resident in the outer membrane of blood leukocytes[1]. The carbohydrate-L selectin

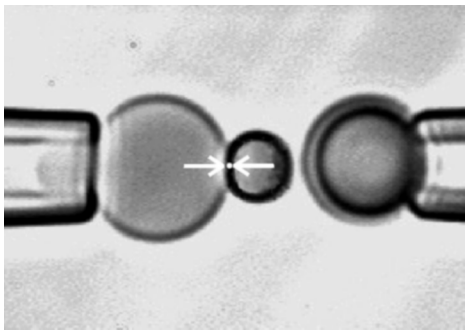

Fig. 1. Operated on the stage of an inverted microscope, the biomembrane force probe BFP is capable of measuring forces from 0.5 to 1000 pN [5]. The BFP spring is a pressurized membrane capsule where membrane tension sets the force constant k_f (force/capsule extension). Controlled by micropipet suction P and radius R_p, the force constant $k_f \sim P \cdot R_p$ can be selected between 0.1 and 3 pN/nm with less than 10% uncertainty using a red blood cell as the transducer. A glass microbead of 1–2 μm diameter is glued to the cell membrane and acts as the BFP tip. To enable this connection, both glass microbeads and red cells are covalently bound with heterobifunctional polyethylene oxide PEG-biotin polymers; microbead surfaces are also bound with monofunctional PEG polymers as a barrier to non-specific adhesion. After reaction with streptavidin, a microbead is pushed against a biotinylated red cell by microrobotic manipulation, which strongly couples the bead to the cell membrane and completes the probe assembly. When required for other molecular attachments to test surfaces, a second ligand is also linked covalently to the probe tip using heterobifunctional PEG polymers. In tests of molecular bond strength, the BFP (seen on the left) is kept stationary and a microbead test surface (on the right) decorated with sites for molecular reaction is translated to/from contact with the BFP tip by precision piezo control. Yielding force, deflection of the transducer is captured at a resolution of 5–10 nm on a fast time scale with high speed (~ 1000 frames/s) video image processing of a narrow scan through the center of the microbead tip. To obtain strength spectra with the BFP technique, detachment forces are measured over a six order of magnitude range in loading rate from 0.1 pN/s to 100 000 pN/s. The loading rate is preselected by choosing the product $k_f v_t$ of transducer force constant k_f and the piezo retraction speed v_t.

[1] Labelled here as *carbohydrate* for convenience, the actual ligand was a short peptide chimera of the biological molecule called *P-selectin glycoprotein ligand* PSGL1, which was made by Genetics Institute and obtained through collaboration with Scott Simon at Baylor College of Medicine.

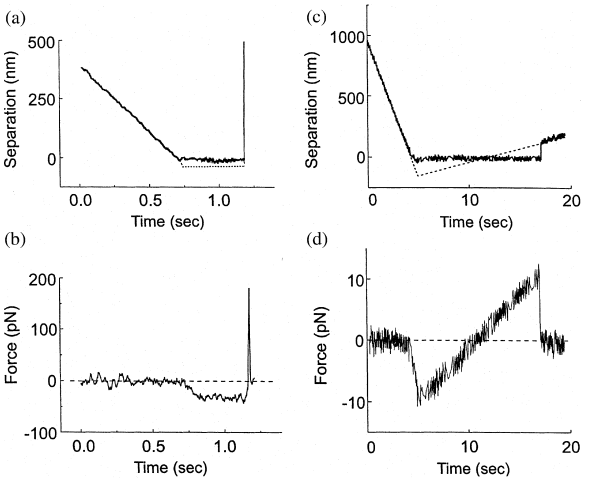

Fig. 2. Figures a,b show the BFP tip-substrate separation and force vs. time for rapid detachment of a single biotin–streptavidin bond. (a) The test microbead was moved towards the probe tip at a speed of ~ 500 nm/s. Stopped for ~ 0.5 s after sensing contact at a preset impingement force of ~ -30 pN, the test surface was then retracted at speed of $\sim 30\,000$ nm/s. (b) Loaded at extremely fast rate, the bond held the tip to the surface for ~ 0.003 s (spike in force) and broke at ~ 180 pN as the piezo continued to retract the test surface. The force fluctuations were due to position uncertainties $\times$ BFP stiffness. (c,d) Shows the BFP tip–substrate separation and force vs. time for a slow detachment of a single biotin–streptavidin bond. (c) The test microbead was moved towards the probe tip at a speed of ~ 200 nm/s. After sensing contact at a preset impingement force of ~ -10 pN, the probe was retracted at slow speed of ~ 10 nm/s. (d) Loaded at very slow rate, the bond held the tip to the surface for ~ 7 s and broke at ~ 10 pN as the piezo continued to retract the test bead (dashed trajectory).

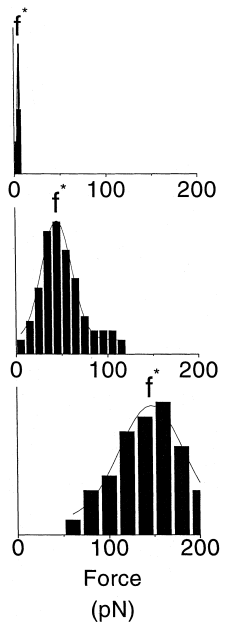

Fig. 3. Examples of force histograms taken from tests of single biotin–streptavidin bonds, which demonstrate shift in peak location and increase in width with increase in loading rate (top histogram — 0.05 pN/s, middle histogram — 20 pN/s, bottom histogram — 60 000 pN/s). Superposed on the histograms are gaussian fits used to determine the most frequent rupture force-bond strength. Governed ideally by the thermal force f_β, standard deviations σ_f of the distributions also reflect uncertainties in position Δx and video sampling time Δt_v, i.e. $\sigma_f \sim [f_\beta^2 + (k_f \Delta x)^2 + (r_f \Delta t_v)^2]^{1/2}$. As σ_f increased from ± 1 pN at the slowest rate to ± 60 pN at the fastest rate, the standard error in mean force — the uncertainty in strength — ranged from ± 0.3 pN to ± 5 pN.

bond is much weaker in affinity with a lifetime of ~ 1 s or less but plays a crucial role in the initial capture of leukocytes from blood circulation at sites of injury or infection [9]. In preparation for each experiment, the appropriate ligand was covalently anchored to a glass microbead along with a chemical glue for attachment of the bead to the BFP transducer (as described in Fig. 1). A similarly-prepared microbead was used as the test surface for probing biotin-(strept)avidin bonds whereas a white blood cell (granulocyte) taken from small blood samples was used as the test surface for probing carbohydrate-L selectin bonds. To ensure that events represented single bonds, the density of reactive sites were reduced significantly so that only one out of 7–10 touches produced a molecular attachment. Also, no nonspecific attachments could be detected when the specific sites were absent. Under this condition, many hundreds of repeated touches were needed to harvest 50 or so detachment forces at loading rates selected in a range between 0.1 pN/s and 100 000 pN/s. Compiled into histograms, Gaussian fits to the distributions were used to locate the peak in each histogram as illustrated in Figs. 3 and 4 which clearly show that the most frequent rupture force shifts upward with loading rate.

Following the same method, the BFP technique was used to probe receptor–lipid anchoring in fluid membranes [4]. As membrane substrates,

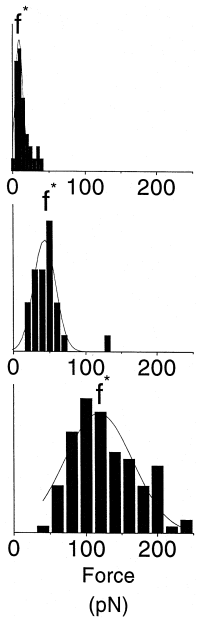

Fig. 4. Examples of force histograms taken from tests of single carbohydrate (sialylated PSGL1 short peptide chimera)-L selectin bonds, which demonstrate shift in peak location and increase in width with increase in loading rate (top histogram — 10 pN/s, middle histogram — 850 pN/s, bottom histogram — 13 000 pN/s). Superposed on the histograms are gaussian fits used to determine the most frequent rupture force-bond strength.

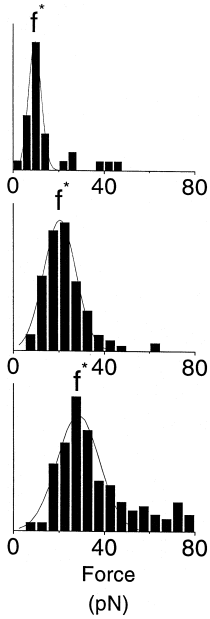

Fig. 5. Examples of force histograms taken from tests of receptor–lipid (biotin-PEG-DSPE) extraction from mixed SOPC/CHOL vesicle bilayers, which demonstrate shift in peak location and increase in width with increase in loading rate (top histogram — 2 pN/s, middle histogram — 200 pN/s, bottom histogram — 5000 pN/s). Superposed on the histograms are gaussian fits used to determine the most frequent extraction force-anchoring strength.

giant bilayer vesicles were prepared with two compositions of lipids: pure stearoyl-oleoyl phosphatidylcholine SOPC (C18:0/1) and a 1:1 mixture of SOPC plus cholesterol (CHOL). As models of receptor lipids, vesicle membranes were doped at extremely low concentration (< 0.0001 mole fraction) with a special biotinylated lipid, biotin-PEG-distearoyl phosphatidylcholine DSPE (diC18:0), kindly provided to us by INEX Pharmaceuticals, Burnaby, BC, Canada. Streptavidin-bound microbeads were used as tips to probe these receptor lipids. The high affinity bond (biotin-streptavidin) enabled the receptor lipids to be extracted from the membrane on separation. Again from many hundreds of repeated touches, histograms of ~ 50–100 detachment forces were compiled at many loading rates and fit with Gaussians to locate the strength peaks as shown by the examples in Fig. 5. The most frequent extraction force shifts upward with loading rate as in the tests of receptor–ligand bond strengths.

3. Theory

3.1. Kinetics of unbinding under force in liquids

In order to appreciate how force and bond survival are related, we briefly review the physics that underlies kinetics of unbinding in a liquid environment, which follows from the seminal work of Kramers 60 years ago [10]. Using Einstein's theory of Brownian motion, Kramers exposed the major impact of viscous damping on kinetics of chemical reactions. For time scales beyond many thermal impulses, overdamped kinetics are modelled by the continuous transport of the density of states $\rho(\boldsymbol{x},t)$ defined at a position $\boldsymbol{x}$ and time t.

Recognized as Smoluchowski's equation [11], changes in the density arise from the divergence of a local flux $\mathbf{J} = D[(\mathbf{f} - \nabla E)\rho/k_BT - \nabla\rho]$, which reflects both convection by force and spread by diffusion. These contributions are scaled by diffusivity D or mobility (D/k_BT) of states and convection is driven by the local gradient in molecular interaction $\nabla E(\boldsymbol{x})$ plus the external force **f**. Although other representations of Brownian dynamics bring out different aspects of the microscopic physics (e.g. the overdamped Langevin equation), Smoluchowski transport readily predicts the rate of thermally-activated escape from a deeply bound state confined by an energy barrier much larger than k_BT.

Starting with all states confined inside the barrier, the kinetics of unbinding are idealized as a stationary flux of probability density ($\mathbf{J}$ = constant in $1-D$ or = constant$/x^{d-1}$ in d-dimensions) along a preferential path from the energy minimum outward past the barrier via a saddle point in the energy surface. In reality, there can be many such paths and the paths can map out complex trajectories in configuration space. However, application of an external pulling force acts to select the reaction path, which we express by a scalar coordinate x. Assumed to be bounded by steeply rising energy in other directions, the energy landscape $E(x)$ along this path is illustrated schematically in Fig. 6a. Governed by orientation θ relative to the microscopic reaction coordinate, external force adds a mechanical potential $-\mathbf{f}\cdot x$ $(\cos\theta)$ that tilts the energy landscape and diminishes the energy barrier E_b at the transition state $(x = x_{ts})$. When the tilted landscape is introduced into the Smoluchowski equation, the stationary solution yields a generic expression for rate of escape from bound to unpopulated-free states under force [1],

$$k_{\text{off}} \approx (D/l_c l_{ts})\exp[-E_b(f)/k_bT]$$

The diffusive dynamics define the attempt frequency $D/l_c l_{ts}$ or diffusion time $t_D = l_c l_{ts}(\gamma/k_BT)$, which is governed by viscous damping γ and two length scales. The length l_c represents the thermal spread in the bound state and defines the entropy gradient $(\partial\rho/\partial x \sim l/l_c)$ that

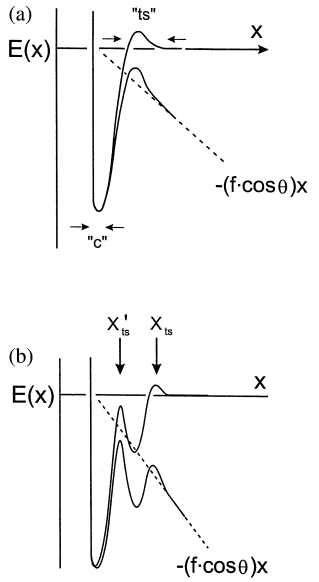

Fig. 6. Conceptual energy landscapes for bound states — 'c' — confined by sharp activation barriers. Oriented at an angle θ to the molecular coordinate x, external force f adds a mechanical potential — $(f\ \cos\ \theta)x$ that tilts the landscape and lowers the barrier. For sharp barriers, the energy contours local to barriers — transition states 'ts' — are highly curved and change little in shape or location under force. (a) A single barrier under force. (b) A cascade of barriers under force. The inner barrier emerges to dominate kinetics when the outer barrier is driven below it by $\geq k_BT$.

drives escape. In a harmonic approximation, l_c is derived from curvature $\kappa_c = (\partial^2 E/\partial x^2)_c$ of the energy landscape local to the minimum, i.e. $l_c = (2\pi k_BT/\kappa_c)^{1/2}$. The other length l_{ts} is the energy-weighted width of the barrier $l_{ts} = \int \mathrm{d}x \cdot \exp[\Delta E(x)_{ts}/k_BT]$ local to the transition state $x = x_{ts}$, which is also determined by curvature $\kappa_{ts} = (\partial^2 E/\partial x^2)_{ts}$ of the energy landscape, i.e. $l_{ts} = (2\pi k_BT/\kappa_{ts})^{1/2}$. For long range potentials, force can displace and narrow the barrier, which introduces a force-dependent prefactor $g(f)$ into the rate expression [i.e. $(\kappa_{ts}/2\pi k_BT)^{1/2} \sim g(f)$]. However, the major impact of force arises in the thermal likelihood of reaching the top of the energy barrier, $\exp[-E_b(f)/k_BT]$. To highlight this feature, the treatment here is restricted to sharp (highly-curved) energy barriers where the shape and location of the transition state are insensitive to external force as illustrated in Fig.

6. Force lowers a sharp barrier by an amount proportional to the thermally-averaged projection[2] $x_\beta = \langle x_{ts} \cos\theta_\beta \rangle$ of the transition state in the direction of force, i.e. $E_b(f) = E_b - f \cdot x_\beta$. Thus, thermal activation introduces a characteristic scale for force given by the ratio of thermal energy to the distance x_β, i.e. $f_\beta = k_B T / x_\beta$. The force f_β can be surprisingly small since $k_B T \approx 4.1$ pN·nm at room temperature and $x_\beta \sim 0.1$–1 nm. The rate of unbinding simply increases exponentially with force, $k_{off} \approx (1/t_o) \exp(f/f_\beta)$, on this scale as postulated by Bell [12] 20 years ago. In contrast to the resonant frequency of bond excitation invoked in Bell's model, Kramers showed that the relevant attempt frequency is $1/t_D = (\kappa_c \kappa_{ts})^{1/2} / 2\pi\gamma$ for overdamped transitions in liquids, which is at least 1000-fold slower. Discounted by the Arrhenius dependence on initial barrier height, the attempt frequency sets the rate scale for spontaneous dissociation, $1/t_o = (1/t_D)\exp(-E_b/k_B T)$.

The model of thermally-activated escape past a single-sharp barrier reveals the intimate relation between force and bond lifetime where bond survival falls e-fold with small increases in force ($= k_B T / x_\beta$) — well below the level of force ($> E_b / x_\beta$) needed for adiabatic rupture of a bond! However, a single barrier is a naive representation of energy landscapes in real biomolecular bonds which have numerous sites of interaction between many small molecules. As such we expect a rough topography of barriers and many possible pathways for unbinding. Again conceptualized as precipitous (sharp) energy maxima along a single pathway, prominent barriers emerge and dominate kinetics in succession as force increases, which is depicted in Fig. 6b. An inner barrier is exposed when force exceeds a crossover level $f_\otimes \approx \Delta E_b / \Delta x_\beta$ set by the splitting ΔE_b between barrier heights and separation in positions Δx_β. Thus, marked by these crossovers, the kinetic rate for unbinding rises in a staircase of force-dependent exponentials [1], which amplify the rate less and less with each increase in thermal force scale as predicted by,

$$k_{off}(f) \approx (1/t_0)\exp\left(f/f_\beta^0\right) / \left\{1 + \sum_{i \to n} l_i \exp\left[(f \cdot \Delta x_\beta - \Delta E_b)_i / k_B T\right]\right\}$$

The transition from one exponential regime to the next depends on the ratio of widths $l_i \approx l_{ts}^i / l_{ts}^o$ $[= (\kappa_{ts}^o / \kappa_{ts}^i)^{1/2}]$ plus differences in location $\Delta x_\beta = x_\beta^o - x_\beta^i$ and energy $\Delta E_b = E_b^o - E_b^i$ of inner barriers relative to the outermost barrier as defined by E_b^o, l_{ts}^o, and x_β^o. The rate of unbinding begins at low force with the steepest exponential dominated by the outermost barrier. At larger forces, the rate crosses over to more shallow exponentials governed by each thermal force scale $k_B T / x_\beta^i$. Thus, a cascade of barriers leads to different levels of strength on different time scales.

3.2. Stochastic process of unbinding in probe experiments

To understand what governs bond strength in probe experiments, we must analyse the stochastic process of bond breakage under steady increase in force. Here, we take advantage of the enormous gap in time scale between ultrafast Brownian diffusion ($t_D \sim 10^{-10}$–10^{-9} s) and the time frame of laboratory experiments ($\sim 10^{-4}$ s to min). The slowly-increasing force in a laboratory test is essentially stationary on the time scale for Brownian diffusion and the frequency of unbinding becomes a variable function of instantaneous force. Thus, the distribution of rupture times can be described in the limit of large statistics by a first-order (Markov) process with time-dependent rate constants [1]. As force rises above the thermal force scale, i.e. $r_f t > k_B T / x_\beta$, the

[2] Forces are sufficient to restrict orientations of the molecules (represented by size L) under thermal fluctuations when $k_B T / L \ll f$. Thus, for large molecules, the thermally-averaged projection x_β of a transition state should remain constant for all forces in excess of the thermal force f_β since $L \gg x_{ts}$ implies $f_? \gg k_B T / L$. Even so, the internal molecular path followed in unbinding may still deviate from the direction of force and experience rapid fluctuations due to excitations of the small scale molecular structure, which is the province of detailed molecular dynamics simulations.

forward transition (unbinding) rate increases extremely rapidly. Also, the molecules drift apart faster than diffusion can recombine them from positions beyond the confining barrier so the reverse rate for rebinding quickly vanishes ($k_{on} \Rightarrow 0$). In this situation, the likelihood $S(t)$ of remaining in the bound state is dominated by the forward process, i.e. $dS(t)/dt \approx -k_{off}(t)\ S(t)$ or equivalently $S(t) = \exp[-\int_{o\to t} k_{off}(t')dt']$. The probability density $p(t) = k_{off}(t)\ S(t)$ for detachment between times t and $t+\Delta t$ describes the distribution of lifetimes. Since instantaneous force is set by time and loading rate ($f = r_f t$), the probability density $p(f)$ for unbinding between forces f and $f+\Delta f$ is equivalent to the distribution of lifetimes $p(t)$,

$$p(f) = (1/r_f)k_{off}(f)\exp \times[-(1/r_f)\int_{0\to f} k_{off}(f')df']$$

because of the statistical identity $p(t)\ dt = p(f)\ df$. The peak in the distribution is the force f^* for most frequent unbinding, which defines strength. Analytically, the location of the peak is found from $\partial p(f)/\partial f = 0$ which establishes a transcendental equation that relates the strength f^* to loading rate r_f,

$$[k_{off}]_{f=f^*} = r_f[\partial \log_e(k_{off})/\partial f]_{f=f^*}$$

In the case of a single-sharp energy barrier, the exponential dependence of unbinding rate on force, $k_{off} \approx (1/t_o)\ \exp(f/f_\beta)$ yields the simple result that strength is linearly proportional to the logarithm of loading rate,

$$f^* = f_\beta \log_e(r_f/r_f^o)$$

with a slope set by the thermal force f_β and introduces an intrinsic-thermal scale for loading rate $r_f^o = f_\beta/t_o$. Similarly, the curvature, $1/\Delta_f^2 = -[1/p(f)][\partial^2 p(f)/\partial f^2]_{f=f^*}$, local to the peak of the distribution can be used to estimate a Gaussian width for uncertainty in the force distribution,

$$1/\Delta_f^2 = \left\{[\partial \log_e(k_{off})/\partial f]^2 - \left[\partial^2 \log_e(k_{off})/\partial f^2\right]\right\}_{f=f^*}$$

Again for a sharp energy barrier, a simple result is found for the spread in force, $\Delta_f = f_\beta$. We see that even in the absence of experimental uncertainty, the force distribution is broadened by thermal activation.

3.3. Dynamic force spectra

Applied to experiment, the signature of a sharp barrier is a straight line in a plot of most frequent probe force f^* against log(loading rate) as illustrated in Fig. 7a. Determined by the ratio of barrier energy E_b to thermal energy k_BT, the linear regime can span orders of magnitude in rate. The slope f_β maps the microscopic transition state to a thermally-averaged distance $x_\beta = \langle x_{ts} \cos \theta_\beta \rangle$ along the direction of force. Barrier energy and the microscopic scale for loading rate f_β/t_D govern the intercept at zero force, $\log_e(r_f^o) = -E_b/k_BT + \log_e(f_\beta/t_D)$. Although a hidden parameter in probe experiments, the microscopic attempt frequency $1/t_D$ is expected to lie in a range from 10^9 to 10^{10} s^{-1} for unbinding in aqueous media (as deduced from molecular dynamics simulations[3]), which introduces a logarithmic bias of $\log_e(t_D) \sim -22 \pm 1$. In other words, the barrier energy can be inferred from the intercept $\log_e(r_f^o)$ at zero force and the slope f_β by, $E_b/k_BT \approx -\log_e(r_f^o) + \log_e(f_\beta) + 22 \pm 1$. This simple relation exposes a unique opportunity to quantitate modifications in energy and/or location of a barrier engineered by point mutations in the binding domain. Since such changes in local molecular structure are not likely to signifi-

[3] The microscopic attempt frequency $1/t_D$ can be estimated using damping factors deduced from MD simulations, which are typically on the order of $\gamma \sim 10^{-8}$ pN-s/nm (equivalent to Stokes drag on a 1-nm size sphere in water), e.g. $\gamma \sim 2\times10^{-8}$ pN-s/nm in simulations of biotin–streptavidin separation [13] and $\gamma \sim 5\times10^{-8}$ pN-s/nm in simulations of lipid extraction from a bilayer [14]. Given that the product of molecular lengths $l_c l_{ts}$ are ~ 0.01–0.1 nm^2, the attempt frequency is expected to be in the range $1/t_D \sim 10^9$–10^{10}/s.

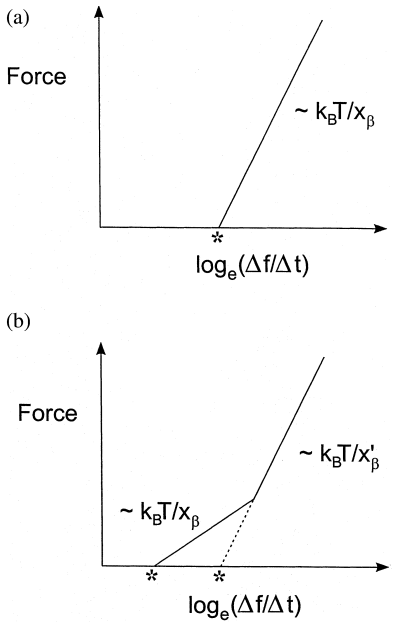

Fig. 7. Dynamic strength spectra for unbinding over sharp activation barriers. Dominated by a specific barrier, the most likely detachment force f^* vs. $\log_e$(loading rate $= r_f$) is a straight line in each regime of the spectrum with a slope $f_\beta = k_BT/x_\beta$ set by the projected location of the barrier x_β along the direction of force. Together with the thermal force f_β, the microscopic attempt frequency $1/t_D$ and height E_b of the activation barrier determine the intrinsic scale for loading rate, i.e. $r_f^o = (f_\beta/t_D)\exp(-E_b/k_BT)$. (a) Spectrum for a single-sharp energy barrier where the logarithmic intercept at zero force (* symbol) can be used to deduce the barrier height given an estimate for the microscopic diffusion time, $E_b/k_BT = -\log_e(r_f^o)^* + \log_e(f_\beta/t_D)$. (b) Piece-wise linear spectrum for a cascade of two sharp energy barriers. The abrupt increase in slope from one thermal force scale to the next shows that the outer barrier has been suppressed and that the inner barrier has become the dominant kinetic impedance to detachment (cf. Fig. 6b). The difference between logarithmic intercepts (* symbols) reflects the splitting in barrier energies adjusted by the ratio of thermal force scales, $\Delta E_b/k_BT \approx -\Delta\log_e(r_f^o)^* + \Delta\log_e(f_\beta)$.

cantly affect the diffusive time scale t_D, changes in barrier energy and/or location can be derived from the shift in the logarithmic intercept and/or change in slope of linear regimes, $\Delta E_b/k_BT \approx -\Delta\log_e(r_f^o) + \Delta\log_e(f_\beta)$. Taken together, these features demonstrate that the plot of most frequent probe force vs. log(probe loading rate) establishes a dynamic spectral image of an activation barrier [1].

Extending this result to more complex energy landscapes, the signature of a cascade of sharp activation barriers is a piece-wise continuous sequence of linear regimes with ascending slopes as sketched in Fig. 7b. The abrupt increase in slope from one regime to the next demonstrates that an outer barrier has been suppressed by force and that an inner barrier has become the dominant kinetic impedance to escape [1]. The dynamic crossovers occur at slightly higher forces than the stationary crossovers ($= \Delta E_b/\Delta x_\beta$) in rate constant as approximated by,

$$f_\otimes^{\mathrm{dyn}} \approx \Delta E_b/\Delta x_\beta + k_BT\left[\log_e\left(x_\beta'/x_\beta\right)\right]/\Delta x_\beta$$

where $\Delta x_\beta = x_\beta{}' - x_\beta$ and $\Delta E_b = E_b{}' - E_b$ are differences between properties of adjacent barriers.

4. Dynamic force spectroscopy of receptor–ligand bonds

Well-recognized in biology, ligand–receptor interactions are the fundament of nanoscale chemistry in recognition, signalling, activation, regulation, and a host of other processes from outside to inside cells. But not well-appreciated in biology is that energy landscapes of receptor–ligand bonds can be rugged terrains with more than one prominent activation barrier. Test-tube assays cannot reveal inner barriers because the slow kinetics depend only on the outermost barrier. However, inner barriers establish different time scales for kinetics under different levels of force, which are imaged by dynamic force spectroscopy. Examining dynamic force spectra for two unrelated receptor–ligand bonds, we will find a similar sequence of three activation barriers but with quite different energy scales. The innermost barrier deep in the binding domain is responsible for the high strength perceived on short time scales and the major portion of total activation energy. The more distal barriers lead to weakness on long time scales but significantly extend bond lifetime in the absence of force. The intriguing question is why did nature create a sequence of time scales for

amplification of kinetics under force in receptor–ligand bonds? Answering this question is likely to introduce a new perspective of biological chemistry.

4.1. Biotin-(strept)avidin bonds

Deduced from a broad distribution of forces, it was concluded in early AFM experiments [15–17] that the strength of a biotin–streptavidin bond was $\sim$200–300 pN and somewhat lower for biotin–avidin $\sim$160 pN. However, as indicated by the force histograms in Fig. 3, the strengths of biotin–streptavidin and biotin–avidin bonds fall continuously from $\sim$200 pN to $\sim$pN with each decade increase in time scale for bond loading from 10^{-3} to 10^{2} s. Plotted in Fig. 8a, the full spectra of strength vs. log(loading rate) exhibit distinct linear regimes, each of which spans 2–4 orders of magnitude increase in loading rate. The abrupt changes in slope reveal a progression of sharp energy barriers that can be easily mapped to positions along the direction of force [2]. Above 85 pN, there is a common high strength regime for both biotin–streptavidin and biotin–avidin with a slope of $f_\beta \approx 34$ pN. This maps a barrier deep in the binding pocket at $x_\beta \approx 0.12$ nm. Below 85 pN, the $f_\beta \approx 8$ pN slope in the biotin–streptavidin spectrum maps the next activation barrier at $x_\beta \approx 0.5$ nm. On the other hand, the steeper slope $f_\beta \approx 13$–14 pN between 38 pN and 85 pN in the biotin–avidin spectrum maps the next barrier to $x_\beta \approx 0.3$ nm and the slight reduction in slope between 38 pN and 11 pN suggests that this intermediate barrier extends to $\sim$0.5 nm. Below 11 pN, the biotin–avidin spectrum exhibits a very low strength regime (dashed line) with a slope of $f_\beta \approx 1.4$ pN that maps to $x_\beta \approx 3$ nm. A similar low strength regime is indicated by results from the slowest test of biotin–streptavidin bonds; but it was not possible to perform tests at loading rates below 0.05 pN/s as needed to verify existence of this regime. In addition to the map of barrier locations, the logarithmic intercepts found by extrapolation of each linear regime to zero force yield the energy differences between activation barriers within each landscape as well as energy differences between related barriers of biotin–avidin and biotin–streptavidin landscapes. To establish a zero reference for energy, we take the logarithmic bias for molecular time scale to be $\log_e(t_D) \sim -22 \pm 1$ for reasons given earlier. With this as the only unknown parameter, the intercept of the high strength regime implies that the innermost barrier is $\sim 20\ k_BT$ above the bound state minimum for both biotin–streptavidin and biotin–avidin bonds. The intercept of the intermediate strength regime sets the next barrier energy $\sim 6\ k_BT$ above the innermost barrier ($\sim 26\ k_BT$ above the bound state) for biotin–streptavidin bonds but only $\sim 3\ k_BT$ above the innermost barrier ($\sim 23\ k_BT$ above the bound state) for biotin–avidin bonds. Lastly, the intercept of the low strength regime sets the energy of the outermost barrier $\sim 7\ k_BT$ above the intermediate barrier ($\sim 30\ k_BT$ above the bound state) for biotin–avidin bonds. The barrier heights and locations projected along the direction of force are sketched in Fig. 8b. The intercept of the lowest strength regime ($\sim$0.0003 pN/s) implies a force-free off rate for biotin–avidin bonds of $\sim 0.4/\text{h}$.[4] This is 20-fold faster than the rate of $\sim 1/55$ h that we measured for spontaneous dissociation of PEG-biotin from streptavidin-bound probe tips in solutions of free biotin and also found in recent studies [8].

Locations of the activation barriers derived from the force spectra can be compared with prominent transition states indicated by molecular dynamics simulations of biotin extraction from streptavidin [13] and avidin [19]. Even with the enormous and fast changes in energy, major transition states are readily identified in simulations by regions of rarified statistics where biotin passes quickly [1]. First, within an initial displacement of 0.1–0.2 nm, extraction forces in both simulations revealed abrupt detachment of biotin from a nest of hydrogen bonds, water bridges, and non-polar

[4] In our tests of biotin–(strept)avidin bond strength, unbinding could occur either by detachment of (strept)avidin from the probe tip or by detachment of biotin linked to the test surface. This introduces a factor of two into the experimental off rate under force so the off rate of a single biotin derived from the intercept of the low strength regime is $\sim 1 \times 10^{-4}$/s.

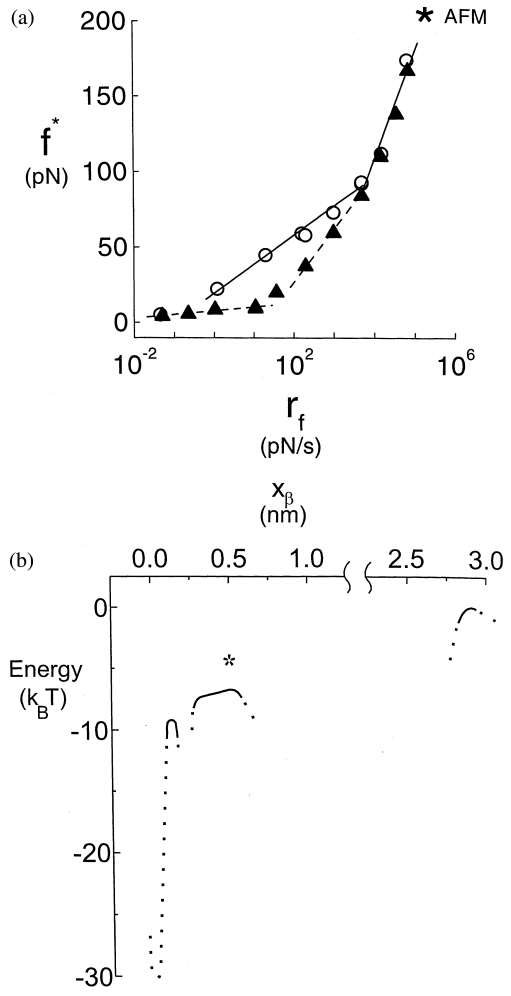

Fig. 8.

interactions deep in the binding pocket. Next, again due to both polar and non-polar interactions, forces reached maximal values followed by sudden displacements of biotin at a distance of ~ 0.4 nm in avidin and ~ 0.5 nm in streptavidin simulations. Clearly, these features correlate well with the dynamic force spectra [2]. Thus, it appears is that the innermost and intermediate transition states implied by the simulations persist on long time scales. However, the outer barrier derived from the low strength regime for biotin–avidin is twofold more distant than the last transition state for avidin in the simulations where biotin was observed to stick to peripheral polar groups at ~ 1.4 nm. This is most likely due to flexibility of the random coil-peripheral loops which border the channel that leads to the binding pocket [20,21].

4.2. Carbohydrate L selectin bonds

In contrast to high affinity biotin–(strept)avidin bonds, carbohydrate-L selectin bonds with modest affinity must stop white cells at vessel walls in the circulation [9]. When arrested suddenly by a bond, the white cell can be subjected to forces of ~ 100 pN in a time frame of milliseconds. Thus, a carbohydrate-L selectin bond would be initially loaded at rates of 10^4–10^5 pN/s. It is useful to keep this functional requirement in mind as we now examine the results from tests of carbohydrate-L selectin bonds [3]. The force spectra are plotted in Fig. 9a. Like biotin–(strept)avidin bonds, we again see a sequence of high — intermediate — and low strength regimes where

Fig. 8 Dynamic strength spectra for both biotin–streptavidin (open circles) and biotin–avidin (closed triangles) bonds [2]. Defined as thermal energy $k_BT \div$ distance x_β, the slopes of the linear regimes seen in the spectra map activation barriers at positions along the direction of force. The common high strength regime in the biotin–streptavidin and biotin–avidin spectra place the innermost barrier at $x_\beta \sim 0.12$ nm. Separate intermediate strength regimes place the next barrier at $x_\beta \approx 0.5$ nm for biotin–streptavidin and $x_\beta \sim 0.3$ nm for biotin–avidin (with a slight reduction in slope below 38 pN suggesting that the biotin–avidin barrier extends to ~ 0.5 nm). Only well-defined in the biotin–avidin spectrum, a low strength regime implies a distal barrier at $x_\beta \approx 3$ nm. Also marked ($\star_{AFM}$) is the biotin–streptavidin strength measured recently by AFM at $\sim 10^5$ pN/s using a carbon nanotube as the tip [18]. This and the earlier measurements of biotin–avidin bond strength [17] at loading rates of $\sim 6 \times 10^4$ pN/s correlate well with the high strength regime shown here. (b) The energy levels of activation barriers derived from the force spectra for biotin–avidin bonds are sketched as a function of distance projected along the direction of force. Differences in barrier energies were obtained directly from the slopes f_β and intercepts r_f^o of each linear regime, $\Delta E_b/k_BT \approx -\Delta \log_e(r_f^o) + \Delta \log_e(f_\beta)$. Providing the absolute scale for energy, the energy minimum (dotted curve) was estimated by taking $\log_e(1/t_D) \sim 22 \pm 1$ to represent the microscopic time scale t_D as described in footnote 2, i.e. $E_b/k_BT = \Delta E_b/k_BT + \log_e(1/t_D)$. The intermediate barrier for biotin–streptavidin bonds is marked by the star (★).

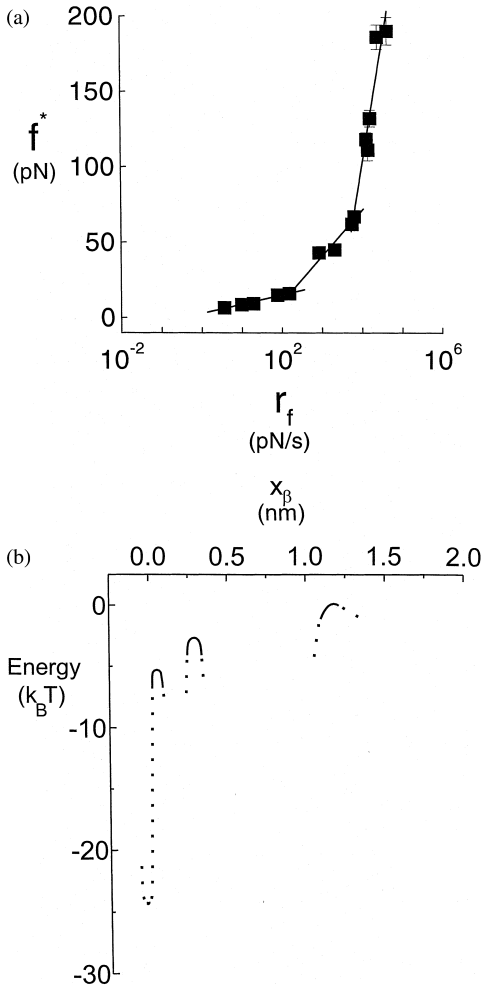

Fig. 9. (a) Dynamic spectrum of strength vs. log(loading rate) for single carbohydrate (sialylated PSGL1 short peptide chimera)-L selectin bonds formed at surfaces of blood granulocytes. Defined as thermal energy $k_BT \div$ distance x_β, the slope of the high strength regime places the innermost barrier at $x_\beta \sim 0.06$ nm. The intermediate strength regime places the next barrier at $x_\beta \approx 0.3$ nm. The low strength regime implies a barrier further out at $x_\beta \approx 1.2$ nm. (b) The energy levels of activation barriers derived from the force spectra are sketched as a function of distance projected along the direction of force. Differences in barrier energies were obtained directly from the slopes f_β and intercepts r_f^o of each linear regime, $\Delta E_b/k_BT \approx -\Delta\log_e(r_f^o) + \Delta\log_e(f_\beta)$. Providing the absolute scale for energy, the energy minimum (dotted curve) was estimated by taking $\log_e(1/t_D) \sim 22 \pm 1$ to represent the microscopic time scale t_D as described in footnote 2, i.e. $E_b/k_BT = \Delta E_b/k_BT + \log_e(1/t_D)$.

strength falls continuously from ~ 200 pN to $\sim$ pN but over fewer decades in time scale from 10^{-3} to 1 s. The high strength regime has a very steep slope of $f_\beta \approx 70$ pN that maps an inner barrier to a small distance $x_\beta \approx 0.06$ nm along the direction of force. Departing from the high strength regime below 70 pN, the intermediate strength regime with a slope of $f_\beta \approx 13$ pN places the next activation barrier at $x_\beta \approx 0.3$ nm. Finally, below ~ 20 pN, the spectrum exhibits a low strength regime with a slope of $f_\beta \approx 3.4$ pN that sets the outermost barrier at $x_\beta \approx 1.2$ nm. Although not shown here, the same barrier locations were obtained from tests of bonds between the same PSGL1 chimera and a chimera of L-selectin bound covalently to microbeads. Thus, the energy landscape derived from the force spectrum is intrinsic to the molecular bond and not influenced by the soft structure of the white blood cell.

As before, extrapolation of each linear regime to zero force yields the differences in energy between activation barriers. Like biotin–(strept)-avidin bonds, the innermost barrier deep in the binding pocket provides strength on short time scales (< 0.03 s), which is sufficient to meet functional requirements noted earlier. Again taking the logarithmic bias for molecular time scale to be $\log_e(t_D)] \sim -22 \pm 1$, the intercept of the high strength regime implies that the innermost barrier is $\sim 18\ k_BT$ above the bound state minimum for carbohydrate-L selectin bonds. The intercept of the intermediate strength regime sets the barrier energy $\sim 3\ k_BT$ above the innermost barrier ($\sim 21\ k_BT$ above the bound state). Lastly, the intercept of the low strength regime sets the energy of the outermost barrier $\sim 3\ k_BT$ above the intermediate barrier ($\sim 24\ k_BT$ above the bound state). Even though only $\sim 6\ k_BT$ higher in energy than the innermost barrier, the outermost activation barrier extends the lifetime of the bond from ~ 0.03 s to ~ 5 s, which is consistent with biochemical properties of carbohydrate-L selectin bonds. The barrier heights and locations projected along the direction of force are sketched in Fig. 9b.

5. Energy landscapes for receptor–lipid anchoring in membranes

Lipids and acylated proteins are anchored in bilayers by hydrophobic interactions, which are characterized by a nearly constant reduction in energy per area of hydrocarbon surface hidden from water [22,23]. Thus, the energy landscape for hydrophobic anchoring of a cylindrical lipid should simply rise linearly with displacement along the bilayer normal. Viewed naively, the model implies that the force to extract a lipid would be set by molecular circumference ($\sim$ radius r_m) and the surface energy per area of water–non-polar exposure, i.e. $f \sim 240$ pN $\times r_m$(nm). Taking a radius ~ 0.5 nm for a lipid, the anchoring force would be ~ 120 pN. However, as indicated by the results in Fig. 5, the strength of lipid anchoring in bilayers is much weaker when lipids are extracted on time scales $> 10^{-3}$ s. Plotted in Fig. 10, the dynamic force spectra obtained from these experiments [4] are consistent with nearly structureless hydrophobic potentials, although a small inner barrier appears in one spectrum. In comparison to the results for receptor–ligand bonds, the forces are much smaller and little structure is seen in the spectra for receptor–lipid anchoring. Over four orders of magnitude in loading rate, only a single linear strength regime is found for extraction of the receptor–lipids from SOPC/CHOL bilayers. The low slope of $f_\beta \approx 2.4$ pN maps a barrier at a distance $x_\beta \approx 1.7$ nm along the direction of force. But revealed by the modest difference in slopes, two linear regimes are found for lipid extraction from pure SOPC bilayers. The initial slope of $f_\beta \approx 3.4$ pN maps an outer barrier at $x_\beta \approx 1.2$ nm and the second slope of $f_\beta \approx 6.1$ pN implies an inner barrier at $x_\beta \approx 0.7$ nm. Consistent with the simple concept of hydrophobic interaction, the locations of the outermost barriers for both types of bilayers are comparable to (but slightly less than) the half thickness of the hydrocarbon region, which is known to increase with cholesterol. This sets a low level for the thermal force scale. Thus, lipid anchoring strength is very weak unless the molecules are extracted extremely rapidly as in molecular dynamics simulations [14]. Still to be studied, integral-membrane proteins are expected to be much more strongly anchored to membranes since interfacial hydrophilic groups will contribute major activation barriers with large thermal force scales.

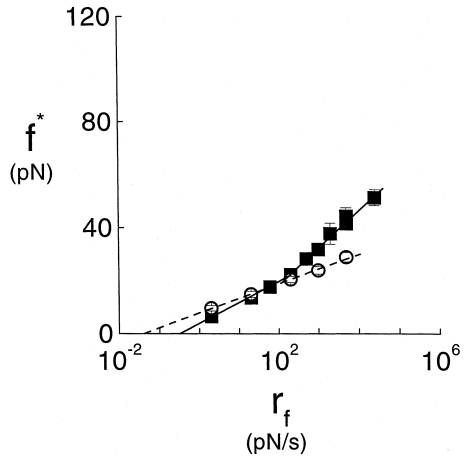

Fig. 10. Dynamic spectra of strength vs. log(loading rate) for extraction of receptor lipids (biotin-PEG-DSPE) from SOPC (closed boxes) and mixed SOPC/CHOL bilayers (open circles). Defined as thermal energy $k_BT \div$ distance x_β, the slopes of the initial linear regimes map activation barriers at $x_\beta \approx 1.2$ nm for extraction from SOPC and $x_\beta \approx 1.7$ nm for extraction from SOPC/CHOL along the direction normal to the bilayer. Not seen in the SOPC/CHOL spectrum, the break in slope for the SOPC spectrum places a weak inner barrier at $x_\beta \approx 0.7$ nm.

As in the analysis of spectra for receptor–ligand bonds, extrapolation of each linear regime to zero force yields the differences in energy between activation barriers. Again taking the logarithmic bias for molecular time scale to be $\log_e(t_D) \sim -22 \pm 1$, the intercept for anchoring strength in SOPC/CHOL bilayers implies that the barrier is $\sim 26\ k_BT$ above the bound state minimum. By comparison, the intercept for anchoring strength in SOPC bilayers implies that the barrier energy is $\sim 24\ k_BT$ above the bound state; the addition of cholesterol increases the outer activation barrier by $\sim 2\ k_BT$. Quite unexpected, the break in slope in the spectrum for SOPC reveals an inner transition state near the middle of the hydrophobic monolayer, which lies $\sim 3\ k_BT$ below the outer barrier. Perhaps coincidental, the location of this inner transition state correlates with the position of the unsaturated bond in the oleoyl

chain of SOPC. Completely speculative, the intermediate activation barrier could indicate that chains feel an entropic bottle-neck as they transiently pass the average position of the unsaturated group. The most puzzling feature is that the intercepts of these spectra at zero force yield only $\sim 0.1-1$ min for lipid residence times in the absence of load. This is much shorter than implied by the lack of perceptible dissociation from an isolated vesicle over the time scale of an hour. Not understood at present, it seems that a soft-outer barrier of a few k_BT must exist which is suppressed by very small forces ($<$ a few pN). Such a barrier could arise from weak association of the lipid acyl chains with the hydrocarbon interstices between head groups at the interface and would extend the residence time by orders of magnitude.

6. Strength of a serial linkage of bonds

It is important to recognize that all attachments involve more than one molecular bond. So what determines the strength of a serial linkage of bonds? We see from Figs. 8–10 that each type of bond has a different force spectrum governed by its molecular energy landscape. Simple comparison of the values of strength at a particular rate shows that one bond is stronger or weaker than another but this hierarchy can be different at a another rate of loading. Naively, we expect strong vs. weak to be defined by the relative heights of the energy barriers that sustain the bonds. However, this criterion is only valid for some sets of bonds; other sets will exhibit unexpected switching amongst the bonds from strong to weak and vice versa as loading rate increases. In the determination of strong vs. weak at a particular loading rate, there are two important parameters: i.e. the spontaneous rates of dissociation set by barrier energies and the thermal force scales that characterize e-fold changes in the frequencies of unbinding under force. With the fast bond (smallest barrier energy) as the reference, the slow bond is defined by differences in barrier energy ΔE_b (>0) and reciprocal thermal force scale $\Delta(1/f_\beta)$ relative to the fast bond. Simple analysis shows that the fast bond is the weak bond when the following inequality holds: $\Delta E_b/k_BT > f\,\Delta(1/f_\beta)$, which is valid for all levels of force if the thermal force scale for the fast bond is less than the thermal force scale for the slow bond [i.e. $\Delta(1/f_\beta) < 0$ or equivalently $\Delta(x_\beta) > 0$]. On the other hand, if the thermal force scale for the fast bond is larger, there is a level of force above which $\Delta E_b/k_BT \leq f\,\Delta(1/f_\beta)$. Unexpectedly, the fast bond becomes the strong bond and the most likely site for failure is the slow bond. In contrast to the image of ascending barriers in a complex bond, the signature of strong to weak bond metamorphosis in a serial linkage of bonds is an abrupt reduction in slope from one linear strength regime to the next as the loading rate is increased. Not only a major factor in cohesive and adhesive strength, switching of the molecular site for failure is likely to be important in biochemical signalling and regulation pathways inside cells.

Acknowledgements

It is important to credit the individuals who carried out the experiments and developed the instrumentation described in this paper. Computer control of the biomembrane force probe assembly and video image processing software were developed by Ken Ritchie (now at Nagoya University in Japan), who also contributed significantly to the theoretical foundations of dynamic force spectroscopy. Tests of biotin–(strept)avidin bonds were performed by Andrew Leung (University of British Columbia) and Pierre Nassoy (now at l'Institut Curie in Paris). Tests of carbohydrate-L selectin bonds were also performed by Andrew Leung in collaboration with Scott Simon (from Baylor College of Medicine in Houston) and Dan Hammer (from University of Pennsylvania in Philadelphia). Tests of lipid anchoring in bilayer membranes were performed by Florian Ludwig (University of British Columbia). The work was supported by grants HL54700 and HL 31579 from the US National Institutes of Health, grant MT7477 from the Medical Research Council of Canada, and the Canadian In-

stitute for Advanced Research Program in Science of Soft Surfaces and Interfaces.

References

[1] E. Evans, K. Ritchie, Biophys. J. 72 (1997) 1541.
[2] R. Merkel, P. Nassoy, A. Leung, K. Ritchie, E. Evans, Nature 397 (1999) 50.
[3] S. Simon, A. Leung, D. Hammer, E. Evans (in review).
[4] F. Ludwig, E. Evans (to be submitted).
[5] E. Evans, K. Ritchie, R. Merkel, Biophys. J. 68 (1995) 2580.
[6] E. Evans, K. Ritchie, Biophys J. 76 (1999) 2439.
[7] N.M. Green, Adv. Protein Chem. 29 (1975) 85.
[8] A. Chilkoti, P.S. Stayton, J. Am. Chem. Soc. 117 (1995) 10622.
[9] T.A. Springer, Annu. Rev. Physiol. 57 (1995) 827.
[10] H.A. Kramers, Physica (Utrecht) 7 (1940) 284.
[11] P. Hanggi, P. Talkner, M. Borkovec, Rev. Mod. Phys. 62 (1990) 251.
[12] G.I. Bell, Science 200 (1978) 618.
[13] H. Grubmuller, B. Heymann, P. Tavan, Science 271 (1996) 997.
[14] S.-J. Marrink, O. Berger, P. Tieleman, F. Jahnig, Biophys. J. 74 (1998) 931.
[15] G.U. Lee, D.A. Kidwell, R.J. Colton, Langmuir 10 (1994) 354.
[16] E.-L. Florin, V.T. Moy, H.E. Gaub, Science 264 (1994) 415.
[17] V.T. Moy, E.-L. Florin, H.E. Gaub, Science 264 (1994) 257.
[18] S.S. Wong, E. Joselevich, A.T. Woolley, C.L. Cheung, C.M. Lieber, Nature 394 (1998) 52.
[19] S. Izrailev, S. Stepaniants, M. Balsera, Y. Oono, K. Schulten, Biophys. J. 72 (1997) 1568.
[20] S. Freitag, I. Le Trong, L. Klumb, P.S. Stayton, R.E. Stenkamp, Protein Sci 6 (1997) 1157.
[21] V. Chu, S. Freitag, I. Le Trong, R.E. Stenkamp, P.S. Stayton, Protein Sci 7 (1998) 848.
[22] D. Marsh, Handbook of Lipid Bilayers, CRC Press, Boca Raton, Fla, 1990, pp. 275–280.
[23] C. Tanford, The Hydrophobic Effect: Formation of Micelles and Biological Membranes, John Wiley & Sons, New York, 1973.